International Journal of Geosynthetics and Ground Engineering (2023) 9:3
https://doi.org/10.1007/s40891-022-00423-w

TECHNICAL NOTE

Analysis of Textured Geomembrane–Soil Interface Strength to Mining Applications

Sergio Luiz da Costa Junior[1] · Maria Alejandra Aparicio-Ardila[1,2] · Carolina Fofonka Palomino[1] · Jefferson Lins da Silva[2]

Received: 14 October 2022 / Accepted: 30 November 2022

Abstract
In mining, due to the high environmental responsibility and the high load supported, the geomembrane-soil interface must guarantee parameters (such as friction angle and adhesion) that contribute to the stability of the barrier system. The use of a textured High-Density Polyethene (HDPE) geomembrane, known as a structured geomembrane, guarantees uniformity in asperity height due to the manufacturing process (flat-die). The present work presents the results of direct shear tests of the geomembrane-soil interface carried out for the liner project of a mining company, where the processing of bauxite, the primary natural source of aluminum, is carried out. The tests were performed with a textured geomembrane with different asperity heights, and two soil types representative of the site (in saturated and dry conditions). The results showed similar values for peak resistance and residual resistance. No influence of the asperity height on the interface parameters was observed, which suggests the need to evaluate other texture characteristics. The need to perform geomembrane-soil interface tests for any liner project, especially for mining, stands out.

Keywords Textured geomembrane · HDPE · Interface shear strength · Asperity height · Mining

Introduction

Aluminium is the third most abundant element in nature. after oxygen and silicon [1]. Aluminium oxide deposits require a hot and humid climate for their formation. Most deposits are located in tropical zones, and their formation is usually associated with laterization phenomena [2]. Alumina is used to produce aluminium metal, whose raw material is bauxite. Obtaining alumina involves extracting the rock (bauxite) that is ground and washed for subsequent chemical treatment. This treatment is essentially done by a process known as the Bayer System, the main industrial method of refining bauxite in the world [3]. At the end of the processing, bauxite residue is generated, an alkaline solid waste known as red mud for the iron oxide present. Generally, in the production of 1 ton of alumina, 1 to 2 tons of bauxite residue are generated. This relationship depends on the quality of the bauxite and the production process [4–6]. Bauxite has its largest reserves in Central and West Africa, Australia, Vietnam and Brazil [7]. According to statistics from the International Aluminium Institute [8], 1,311,089.5 thousand metric tonnes of alumina were produced in the last ten years, of which 93.95% metric tonnes of alumina were used in the production of aluminium (metallurgical grade). China was responsible for producing 54.36% metric tonnes of alumina; in the South America region, an average of 2.41% of metric tonnes of alumina was produced. The bauxite residue distribution is consistent with alumina and is relatively concentrated worldwide [9].

The disposal and storage of mining waste is a geotechnical challenge since these materials exhibit considerable variability in their physical–chemical and mineralogical characteristics [10]. Waste of this type presents a high risk of environmental impact in the case of accidents such as bauxite residue. High-density polyethene (HDPE) geomembranes are used as liquid and gas barriers in various geotechnical and environmental applications [11], such as mining's. In Brazil, there is a technical standard ABNT 16,199 [12] and a technical recommendation of the

✉ Maria Alejandra Aparicio-Ardila
maparicio@usp.br

[1] Nortene Group, Alphaville, São Paulo 06455-050, Brazil

[2] São Carlos School of Engineering (EESC), University of São Paulo (USP), São Carlos, São Paulo 13566-590, Brazil

Published online: 17 December 2022

International Geosynthetics Society—IGS Brazil [13], concerning geomembrane installation practice [14]. The HDPE geomembrane manufacturing process involves mixing polyethene resin, carbon black and antioxidants/stabilizers, which are sent to an extruder (to melt). It is then mixed to give a homogeneous distribution and dispersion. The molten resin is forced through a flat-die or round-die (blown-film) [15–17]. Geomembrane texturing techniques vary from manufacturer to manufacturer. The technique influences the microtexture's and macrotexture's strength and durability of the geomembrane [18].

The most used methods to texturize geomembranes are: structuring (by flat-die) and coextrusion (by round-die). The coextrusion method uses nitrogen as the blowing agent. The texture is formed by the shear action of the extruder, which breaks the bubbles formed by nitrogen cooling. This process depends on the extrusion rate. On the other hand, the structuring process forces an extruded geomembrane on the flat-die through two counter-rotating rollers with patterned surfaces [19]. The structured geomembrane is uniform compared with the coextruded geomembrane. It is noteworthy that although the geomembrane is manufactured on the same machine and with the same resin, each manufacturing batch has different thermal and stress histories that can affect its morphological structure and, therefore, affect both the final properties and the rate of degradation [17].

The textured HDPE geomembrane is widely used in works with high environmental responsibility because it increases the friction characteristics and the safety factor, reducing the risk of ruptures due to slipping between interfaces. In liner works, interface friction is a critical design parameter to analyse the deposited residue's stability. Interface friction tests measure the shear strength necessary to keep interfaces and materials intact when agents such as gravity require them. Several studies have been carried out analysing the behaviour of the interface between geomembrane-soil and geomembrane-geosynthetics (such as geotextile and GCL) [19–22].

A geomembrane installed over a layer of soil generates a contact zone between the materials. In this contact zone, a force that prevents the relative movement between the two materials is called shear force. This contact shear strength is a function of the friction angle between the two materials. This parameter depends on the characteristics of both: the soil (granulometry, moisture content, degree of compaction, among others) and the geomembrane (raw material and texture of the material), in addition to external factors such as temperature and percolating liquid. Several authors report different friction and adhesion angle values between different types of soils and HDPE geomembranes obtained by shear tests with direct shear box and inclined board test results and with different box sizes [23–29].

The most commercialized textured geomembrane is the coextruded geomembrane. However, it has not provided acceptable results in terms of surface texture, presenting varying texture heights, questionable geomembrane quality and decreased tensile strength. Additionally, during installation, the coextruded geomembrane has a problematic "velcro effect" adhesion that requires careful positioning or a skid plate. In contrast, the structured geomembrane allows easy geotextile, GCL and geocomposite placement [30, 31]. In recent years, the use of structured textured geomembranes has increased due to their better performance than coextruded ones. The present work presents the results of geomembrane-soil interface shear tests. The tests were carried out with samples of structured textured geomembranes with different asperity heights to analyse the geomembrane-soil interface for a bauxite mining project located in the state of Maranhão—Brazil. The main interface parameters analysed were: soil-geomembrane interface friction angle, soil-geomembrane adhesion, two soil types, and saturated/dry soil condition. The main objective of this work is to provide design data for mining works using textured geomembranes.

Materials and Methods

Study Area

The work involved adapting several areas to dispose of bauxite residue in the state of Maranhão, northern Brazil. In the study area, nine dams with an average height of 13 m were built through clay soil compaction above the natural soil, Fig. 1 shows the typical cross-section of the dam.

The project presented the following challenges: Risk of contamination of nearby water resources (the work is located 10 km from São Marco Bay and 2.5 km from Arraial Bay) and risk of geotechnical instability caused by possible soil liquefaction of the foundation.

The local soil is fine red and yellow silty sand over 6.0 m thick. Two different soil samples were used in this study, Soil 1 was collected at a depth of 1.00–1.50 m at the foundation of the work, Soil 2 was collected later in a different region. Table 1 presents soils characteristics. Figure 2 shows the extraction of undisturbed soil samples.

The graph in Fig. 3 shows the granulometric curves of Soil 1 and Soil 2. In the same graph, the liquefaction intervals established by Tsuchida [37] can be observed. The interval defined by the black dashed lines indicates soils susceptible to liquefaction, and the interval between the dashed red lines indicates soils more susceptible to liquefaction, Fig. 3 shows that both soils are between the intervals established by Tsuchida [37], indicating that both soils are susceptible to liquefaction.

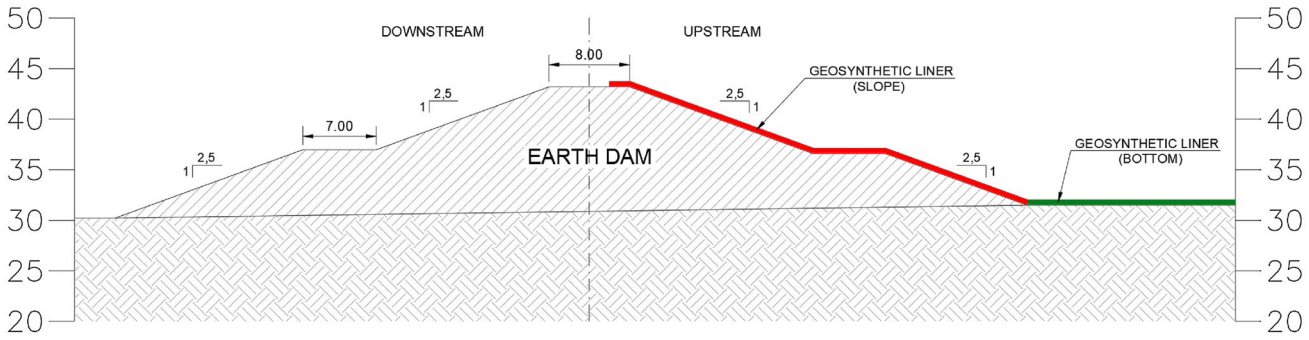

Fig. 1 Typical cross section

Table 1 Soil 1 and Soil 2 characteristics

Properties	Test method	Soil 1	Soil 2
Plastic Limit—PL	NBR 7180 [32]	Non-plastic	Non-plastic
Liquid Limit—LL	NBR 6459 [33]	Non-liquid	Non-liquid
Particle size distribution	NBR 7181 [34]	Silt–clay sand	Silt–clay sand
USCS classification	ASTM D2487 [35]	SM	SM
Maximum dry density- (γd)	NBR-7182 [36]	1.87 g/cm^3	2.10 g/cm^3
Optimum water content	NBR-7182 [36]	9.8%	6.8%

Fig. 2 Undisturbed sample of Soil 1 (*Left*) and Soil 2 (*right*)

Due to the presence of fine sand (with high permeability) in the foundation of the work, the percolation of bauxite residue could generate both environmental contamination and geotechnical instability by liquefaction. Because of this, a double liner was installed for the dam lining system to dispose of bauxite residue. According to the recommendation of IGS Brasil [13], a double sealing device consists of the superposition of two active sealing elements, that is, two geomembranes. Two textured 1.5 mm geomembrane layers with an intermediate Geosynthetic Clay Liner (GCL) layer was designed. In addition, on the slopes, it was installed a geotextile layer and geocell filled with concrete (Fig. 4a). A drainage geocomposite and a layer of compacted clay were installed at the bottom of the reservoir, as seen in Fig. 4b. The present study focuses on the analysis of the foundation soil and geomembrane interface.

Geomembrane

Nine geomembrane samples (GM) manufactured from the structuring process with asperity heights between 0.52 mm and 1.00 mm were used. All the samples are textured on both sides. The geomembranes characteristics are presented in Table 2. The samples used were manufactured

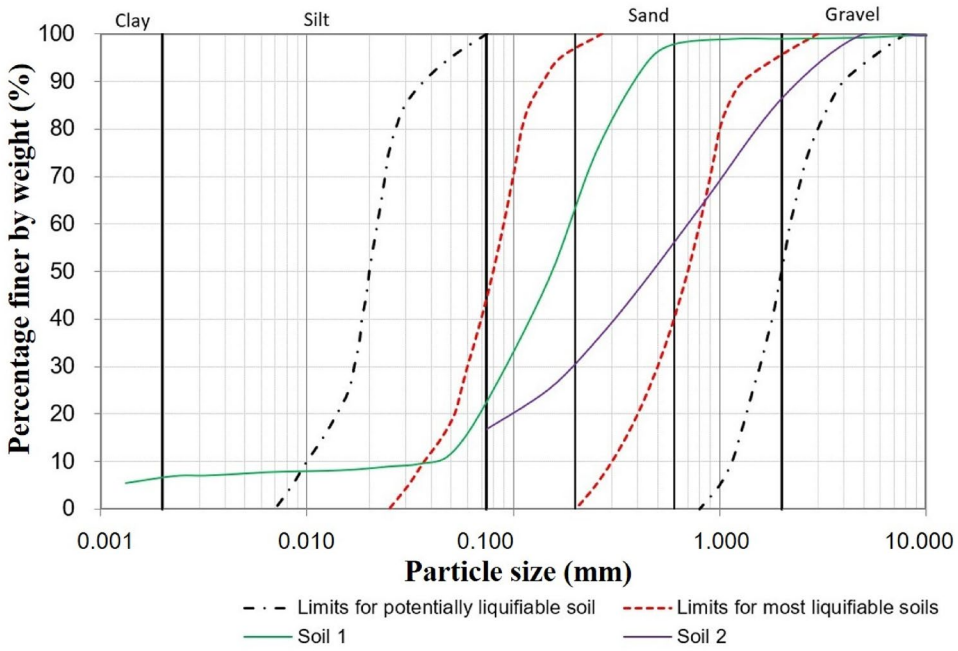

Fig. 3 Liquefaction intervals and granulometric curves of Soil 1 and Soil 2

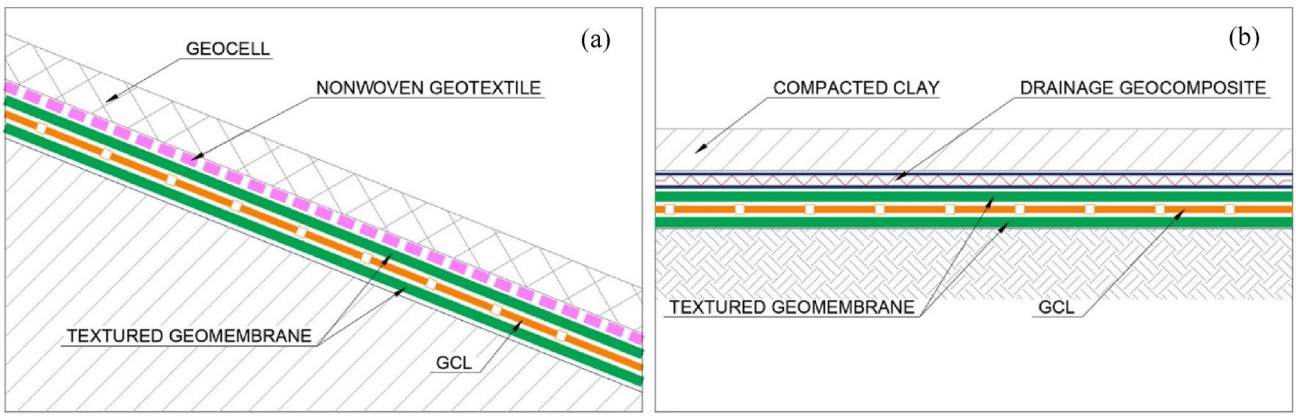

Fig. 4 Geosynthetic Liner: **a** slope and **b** bottom

in three manufacturing batches, grouped as follows: Batch 1 (GM1 e GM2), batch 2 (GM3, GM4 e GM5) and batch 3 (GM6, GM7, GM8 e GM9).

All analysed geomembranes meet the GM13 [38] recommendations, as the asperity height is greater than 0.4 mm. The geomembrane characterization tests were carried out in the Geosynthetic Laboratory at the University of São Paulo (USP) in São Carlos, state of São Paulo, Brazil. Figure 5 shows a sample of the geomembranes used.

The results show that asperity height also influences other mechanical parameters such as break strength, yield strength, break elongation, tear resistance and puncture resistance, as can be seen in Table 2.

Test Procedures

The Interface Soil Geomembrane tests (ISG) for determining the shear strength were performed following the ASTM D5321 standard [48]. A 300×300 mm wide box was used to determine the interface parameters (adhesion and interface friction angle). Figure 6 presents a schematic of the equipment used for the direct shear test.

The load was applied to the soil for at least one hour before the test was carried out, and the loading ranges adopted were from 5 to 50 kPa. The ISG tests with GM1 (ISG-1) and GM3 (ISG-3) were conducted in the dry condition, while the other tests were carried out in the saturated

Table 2 Geomembranes properties

Properties	Test method	GM1	GM2	GM3	GM4	GM5	GM6	GM7	GM8	GM9
Asperity height (mm)	ASTM D7466 [39]	0.93 (±0.03)	1.00 (±0.03)	0.84 (±0.07)	0.78 (±0.06)	0.88 (±0.05)	0.86 (±0.04)	0.93 (±0.07)	0.52 (±0.04)	0.59 (±0.03)
Thickness (mm)	ASTM D5994 [40]	1.53 (±0.01)		1.47 (±0.01)			1.47 (±0.01)			
Density (g/cm^3)	ASTM D1505/D792 [42.43]	0.949 (±0.002)		0.949 (±0.001)			0.948 (±0.001)			
Break strength (kN/m)	ASTM D6693 [43]	33.99 (±1.84)		36.15 (±3.71)			32.06 (±0.78)			
Yield strength (kN/m)		30.37 (±1.49)		27.88 (±0.42)			28.44 (±0.43)			
Break elongation (%)		411.99 (±35.38)		513.58 (±63.05)			386.30 (±40.08)			
Yield elongation (%)		15.48 (±0.41)		15.27 (±0.32)			16.77 (±0.42)			
Tear resistance (N)	ASTM D1004 [44]	252.40 (±5.36)		240.01 (±4.01)			244.55 (±3.64)			
Puncture resistance (N)	ASTM D4833 [45]	685.83 (±13.16)		637.57 (±22.04)			699.69 (±4.31)			
Carbon black content (%)	ASTM D4218 [46]	2.73 (±0.16)		2.41 (±0.09)			2.31 (±0.16)			
Oxidative induction time—OIT (min)	ASTM D8117 [47]	169.02 (±7.44)		193.38 (±6.82)			225.21 (±0.01)			

Standard deviation in brackets

condition to provide design parameters under different conditions. The displacement rate for all the tests was about 1.0 mm/min, and the horizontal displacement was monitored every half millimeter. The maximum horizontal displacement allowed by the equipment was up to 75 mm.

The geomembrane is positioned between the mobile and fixed boxes to guarantee the contact of the geomembrane textures with the compacted soil of the upper box. O Soil 1 was remolded to 98% of the maximum dry density at the optimum moisture content, and Soil 2 was compacted at 9.0% water content and 20.8 kN/m^3.

The highest shear stress values found in the stress curves by horizontal displacement were considered to determine the peak parameters. The last values found in the displacement stress curve of each load were considered for the residual values. The interface resistance envelope was obtained from linear regression, with the adhesion value meeting the trend line with the ordinate axis (y) and the interface friction angle as the straight-line slope.

Results and Discussion

Figure 7A–d show the shear strength soil-geomembrane versus horizontal displacement curves considering confining stresses of 5, 10, 20 and 50 kPa. The tests with the GM1 to GM5 geomembranes were performed with type 1 soil, and the other GM6 to GM9 geomembranes used type 2 soil. The ISG-1 and ISG-3 tests were carried out in dry condition, corresponding to the GM1 and GM3 geomembranes. In the saturated condition, the tests ISG-2, ISG-4, ISG-5, ISG-6, ISG-7, ISG-8 and ISG-9 were carried out, which correspond to the geomembranes GM2, GM4, GM5, GM6, GM7, GM8 and GM9. Figure 7a, d show that there was no standard behavior considering the types of geomembranes that differ mainly by asperity height. The 5 kPa confining stress test was not performed on the GM8 geomembrane (ISG-8).

The geomembranes showed peak and residual strength, and the curve profile was maintained for each geomembrane, as seen in the GM3 geomembrane (ISG-3). Residual strengths were obtained with displacements more significant than 5 mm; in some cases, the shear strength continued to increase until the end of the test. Based on the Mohr–Coulomb theory, it was possible to obtain the interface shear strength envelope from the interface shear strength vs displacement curves. They were obtained by fitting linear regression lines.

The interface shear strength envelopes for geomembrane-soil interfaces, under different conditions, are shown in Fig. 8. The interface friction angle and adhesion, for each test, were obtained from the linear regression lines, their values are shown in Table 3.

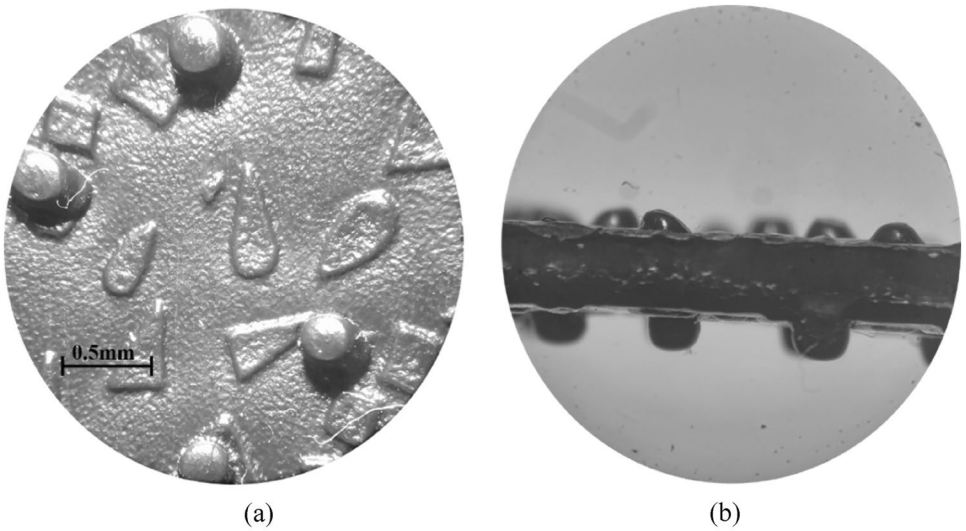

Fig. 5 HDPE textured geomembranes samples (magnification: 10×). **a** Standard textured surface and **b** cross-sectional view of two-sided textured geomembrane

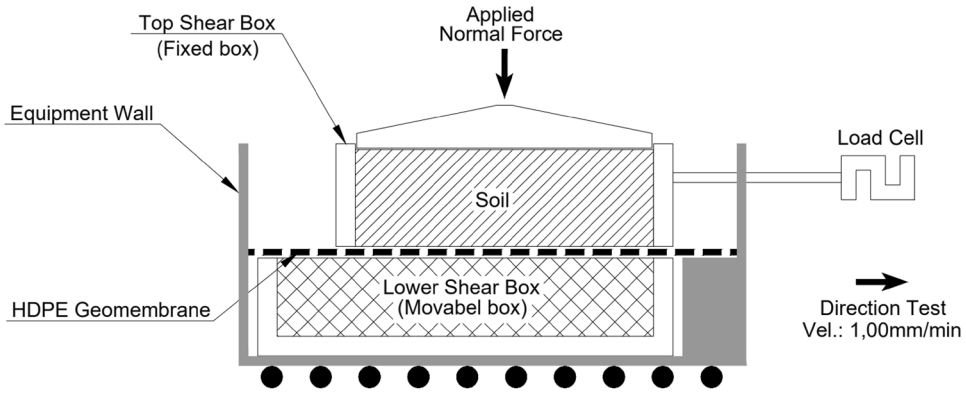

Fig. 6 Scheme of direct shear test

Soil 2 presents in its composition particles with larger diameters than soil 1, the values of interface friction angle found in the tests carried out with soil 2 were higher.

In general, the presence of water in the tests reduced the values of interface friction angles. The tests carried out in dry condition (ISG-1 and ISG-3). with Soil 1, presented values of peak interface friction angles higher than those carried out in the saturated condition. However, there was no interference of water in the residual parameters. In this study, tests with smooth geomembranes were not performed. As it is known, textured geomembranes present higher values of the parameters of the geomembrane-soil interface. A fact supported by the results widely disseminated in the literature [19–29]. In addition, was used a structured geomembrane, which presents uniformity in asperity height. Opposed to the observed in a coextruded geomembrane.

The values of the soil-geomembrane interface parameters showed similar values for the peak and residual resistance, showing no substantial increase or decrease in the typical curves, as can be seen in Fig. 7. Finally, the different asperity heights did not significantly influence the interface strength parameters. When comparing the ISG-9 interface, which has an asperity height of 0.59 mm, with the ISG-6 (asperity height = 0.86 mm) and ISG-7 (asperity height = 0.93 mm) interfaces, all tested with Soil 2. It was possible to verify that there was no significant change in interface friction and adhesion angle values. Other characteristics must be considered in the performance of textured geomembranes, as the spacing of asperities and the presence or absence of micro and macro asperities.

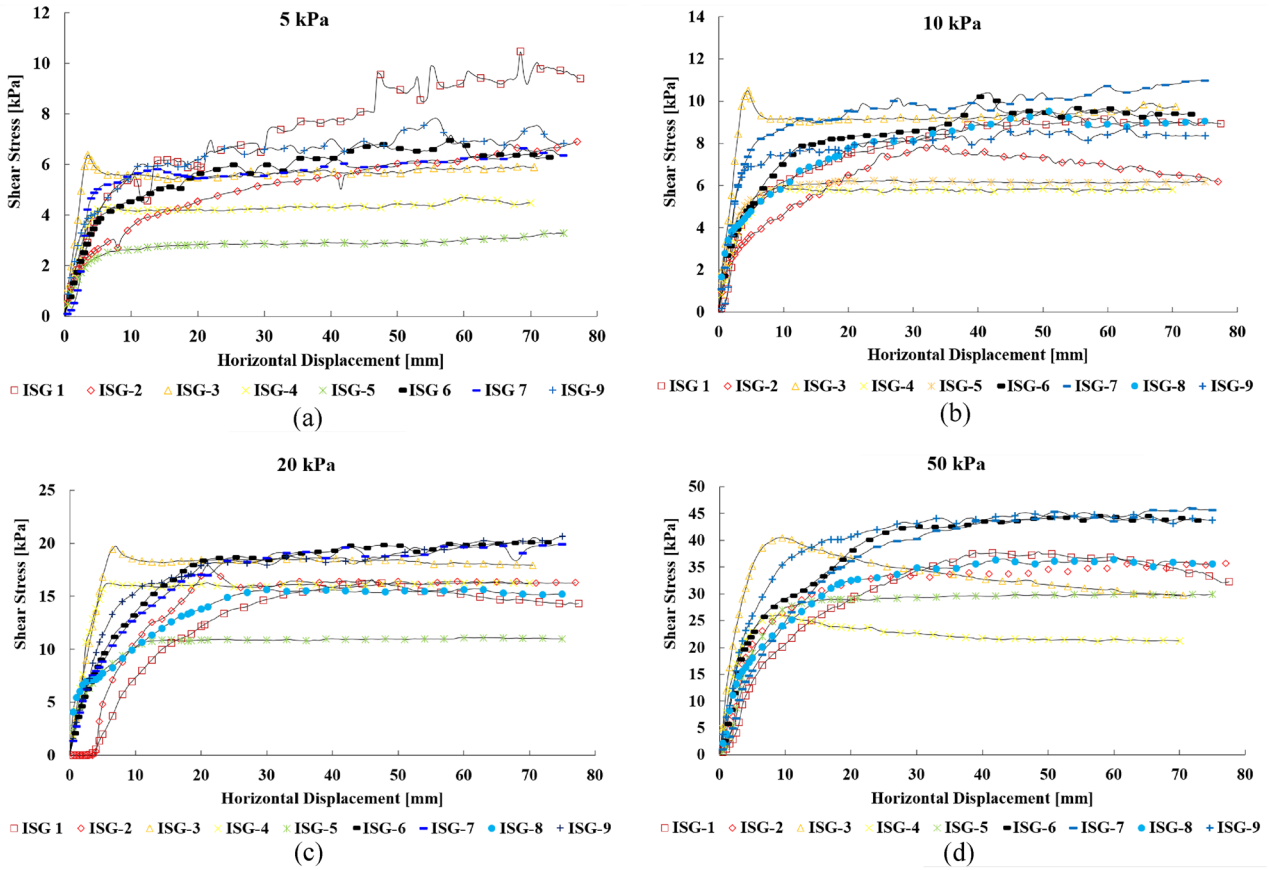

Fig. 7 Interface shear strength vs horizontal displacement

Conclusions

Based on the result of this study. the following conclusions were drawn:

- The shear strength of the textured geomembrane interface depends on the asperity height, soil type, normal load and saturation condition of the soil. Soil 1 has smaller particles than soil 2, and the interface friction is smaller for soil 1. In the presence of water, there was no influence on the residual resistance parameters, but the friction angle of peak resistance increased.
- The results showed that the asperity height influences the geomembrane strength parameters, including break strength, yield strength, break elongation, tear resistance and puncture resistance.
- The results showed that the asperity height did not significantly influence the soil-geomembrane interface strength parameters, which may be related to the soils used in the present study (with similar characteristics). It is recommended for future work to use soils with both clayey and sandy characteristics.
- In addition to the asperity height. the spacing of the asperities, and the presence or absence of micro and macro asperities must be considered in the geomembrane-soil interface.

The study showed the need to perform geomembrane-soil interface tests for any liner project, mainly for mining and sanitary landfills.

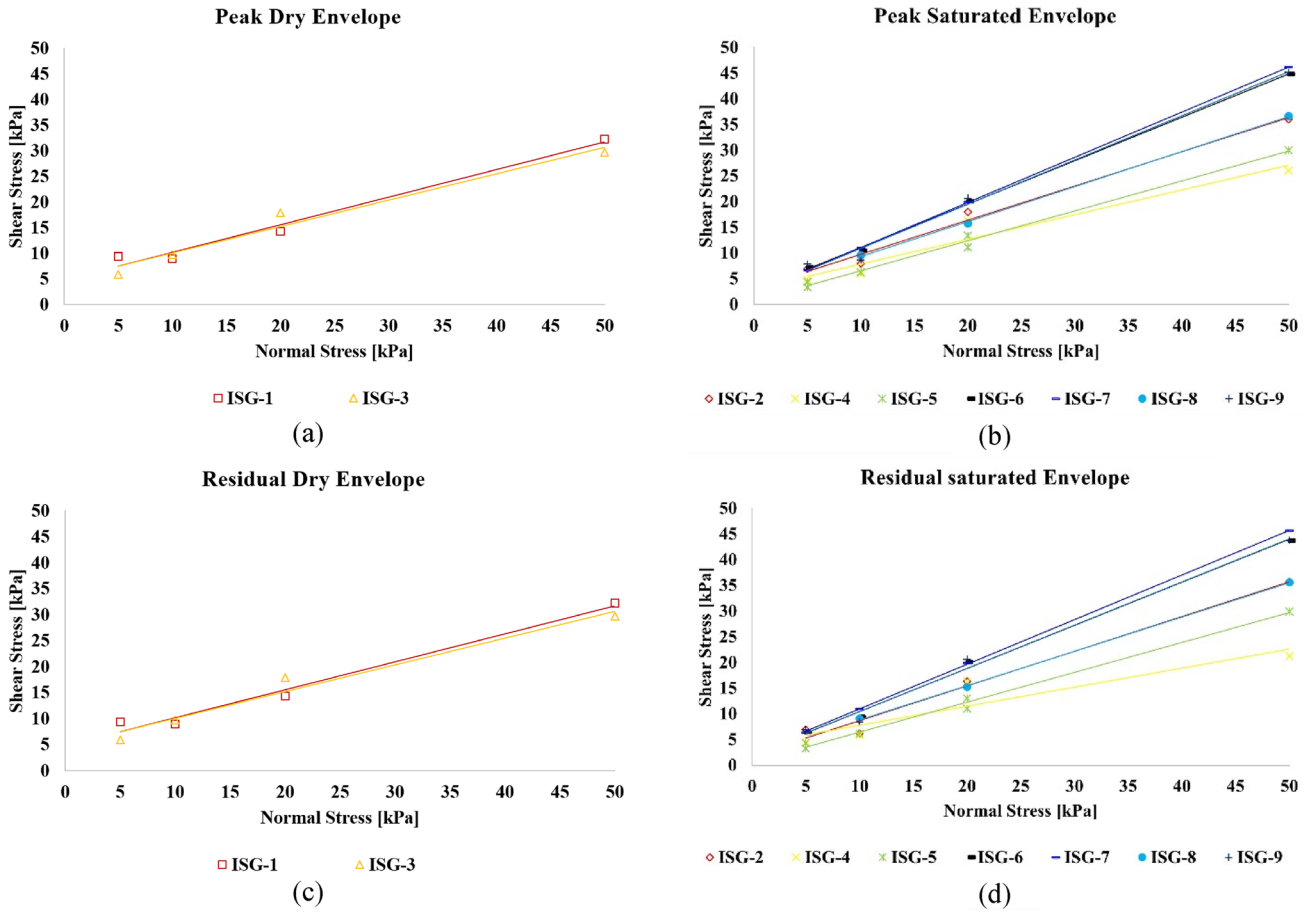

Fig. 8 Interface shear strength envelopes

Table 3 Interface geomembrane-soil parameters

Interface	Soil	Geomembrane	Asperity height (mm)	Peak		Residual	
				Adhesion (kPa)	Interface Friction angle (º)	Adhesion (kPa)	Interface friction angle (º)
ISG-1	1 (dry)	GM 1	0.93	4.8	33.0	4.8	28.3
ISG-2	1 (saturated)	GM 2	1.00	3.1	33.6	1.9	34.1
ISG-3	1 (dry)	GM 3	0.84	3.3	37.0	4.9	27.2
ISG-4	1 (saturated)	GM 4	0.78	3.0	25.6	4.1	20.4
ISG-5	1 (saturated)	GM 5	0.85	0.7	30.2	0.6	30.2
ISG-6	2 (saturated)	GM 6	0.86	2.7	40.2	2.0	40.0
ISG-7	2 (saturated)	GM 7	0.93	2.2	41.3	2.2	41.0
ISG-8	2 (saturated)	GM 8	0.52	2.5	34.2	2.2	33.7
ISG-9	2 (saturated)	GM 9	0.59	2.3	40.7	2.0	40.1

Batch 1 (GM1 e GM2). batch 2 (GM3. GM4 e GM5) and batch 3 (GM6. GM7. GM8 e GM9)

Acknowledgements The authors would like to thank the Nortene group for providing the data.

Author contributions The individual contributions of each author are highlighted as follows: SLdCJ: methodology. data analysis. validation. and writing (original draft); MAA-A: conceptualization. methodology. investigation. and writing (original draft); CFP and JLS: conceptualization. project administration. resources. supervision. methodology. funding acquisition and resources. writing (reviewing and editing).

Funding This research was funded in part (support granted to the second author) by the Brazilian Federal Agency for Support and

Evaluation of Graduate Education (Coordenação de Aperfeiçoamento de Pessoal de Nível; CAPES)-Finance Code 001.

Availability of data and material The data presented in this study are available on request from the corresponding author.

Code availability Not applicable.

Declarations

Conflict of Interest The authors declare that they have no conflict of interest.

References

1. Sampaio JA, Andrade MCD, Dutra AJB (2005) Bauxita. In: CETEM/MCT (in Portuguese)
2. Bogatyrev BA, Zhukov VV (2009) Bauxite provinces of the world. Geol Ore Depos 51(5):339–355
3. Khairul MA, Zanganeh J, Moghtaderi B (2019) The composition. recycling and utilisation of Bayer red mud. Resour Conserv Recycl 141:483–498
4. Zhao Y, Wang J, Luan Z, Peng X, Liang Z, Shi L (2009) Removal of phosphate from aqueous solution by red mud using a factorial design. J Hazard Mate 165(1–3):1193–1199
5. Borra CR, Pontikes Y, Binnemans K, Van Gerven T (2015) Leaching of rare earths from bauxite residue (red mud). Miner Eng 76:20–27
6. Borra CR, Blanpain B, Pontikes Y, Binnemans K, Van Gerven T (2016) Recovery of rare earths and other valuable metals from bauxite residue (Red mud): a review. J Sustain Metall 2:365–386
7. Summaries MC (2021) Mineral commodity summaries. US Geological Survey, Reston
8. Aluminium W (2022) Alumina Production. In: International Aluminium Institute, London
9. Lyu F, Hu Y, Wang L, Sun W (2021) Dealkalization processes of bauxite residue: a comprehensive review. J Hazard Mater 403:123671
10. Reddy PS, Reddy NG, Serjun VZ, Mohanty B, Das SK, Reddy KR, Rao BH (2021) Properties and assessment of applications of red mud (bauxite residue): current status and research needs. Waste Biomass Valorization 12(3):1185–1217
11. Rowe RK (2005) Long-term performance of contaminant barrier systems. Geotechnique 55(9):631–678
12. Associação Brasileira de Normas Técnicas, ABNT NBR 16199:2020 (2013) Barreiras geossintéticas—Instalação de geomembranas poliméricas; Rio de Janeiro (in Portuguese)
13. Associação Brasileira de Geossintéticos. Recomendação IGS Brasil 004-2016 (2016) Aplicação de Geossintéticos em Áreas de Disposição de Resíduos. São José dos Campos (in Portuguese)
14. Lavoie FL, Kobelnik M, Valentin CA, da Silva JL (2020) Durability of HDPE geomembranes: an overview. Quim Nova 43:656–667
15. Struve F (1994) Extrusion of geomembranes. Proceedings of the 8th GRI Conference. Geosynthetic Resins. Formulation and Manufacturing. In: Hsuan G, Koerner RM (eds) Industrial FabricsAssociation International (IFAI), St Paul, pp 94–112
16. Scheirs J (2009) A guide to polymeric geomembranes: a practical approach. Wiley, Hoboken
17. Ewais AMR, Rowe RK (2014) Effects of blown film process on initial properties of HPDE geomembranes of different thicknesses. Geosynth Int 21(1):62–82
18. Frost JD, Evans TM, Hebeler GL, Giroud JP (2002) Influence of wear mechanisms on geosynthetic interface strengths. In: Proceedings of the Seventh International Conference on Geosynthetics, Nice, France, vol. 4, pp 1325–1328
19. Hebeler GL, Frost JD, Myers AT (2005) Quantifying hook and loop interaction in textured geomembrane–geotextile systems. Geotext Geomembr 23(1):77–105
20. Stark TD, Williamson TA, Eid HT (1996) HDPE geomembrane/geotextile interface shear strength. J Geotech Eng 122(3):197–203
21. Jones DRV, Dixon N (1998) Shear strength properties of geomembrane/geotextile interfaces. Geotext Geomembr 16(1):45–71
22. Li MH, Gilbert RB (1999) Shear strength of textured geomembrane and nonwoven geotextile interfaces. In: Proceedings of Geosynthetics '99, vol 1, IFAI, Boston, pp. 505–516
23. Rigo JM, Rollin AL (1990) Geomembranes-identification and performance testing. CRC Press
24. O'rourke TD, Druschel SJ, Netravali AN (1990) Shear strength characteristics of sand-polymer interfaces. J Geotech Eng 116(3):451–469
25. Koerner RM (1998) Design with geosynthetics, 4th edn. Prentice Hall, Hoboken
26. Sharma HD, Lewis SP (1994) Waste containment systems waste stabilization and landfills: design and evaluation. Wiley, New York
27. Izgin M, Wasti Y (1998) Geomembrane–sand interface frictional properties as determined by inclined board and shear box tests. Geotext Geomembr 16(4):207–219
28. Lopes PC, Lopes ML, Lopes MP (2001) Shear behaviour of geosynthetics in the inclined plane test—influence of soil particle size and geosynthetic structure. Geosynth Int 8:327–342
29. Markou INE, ED, (2018) Shear resistance characteristics of soil–geomembrane interfaces. Int J Geosynth Ground Eng 4(4):1–16
30. Froble R (2007) Using structured geomembranes in final solid-waste landfill closure designs. Geosynthetics 25(1):12–18
31. Palmeira EM, Tatsuoka F, Bathurst RJ, Stevenson PE, Zornberg JG (2008) Advances in geosynthetics materials and applications for soil reinforcement and environmental protection works. Electron J Geotech 13:1–38
32. ABNT NBR 7180 (2016) Soil–plasticity limit dertermination. Brazilian Association of Norms Techniques
33. ABNT NBR 6459 (2017) Soil–liquid limit determination. Brazilian Association of Norms Techniques.
34. ABNT NBR 7181 (2018) Soil–Grain size analysis. Brazilian Association of Norms Techniques.
35. ASTM International (2017) ASTM D2487. Standard Practice for Classification of Soils for Engineering Purposes (Unified Soil Classification System). In: ASTM International, West Conshohocken, Pennsylvania, USA
36. ABNT NBR 7182 (2020) Soil—compaction test. Brazilian Association of Norms Techniques
37. Tsuchida H (1970) Prediction and Countermeasure against Liquefaction in Sand Deposits. Abstract of the Seminar of the Port and Harbour Research Institute. Ministry of Transport. Yokosuka, Japan, pp 3.1–3.33 (In Japanese)
38. GRI - GM13 (2021) Test methods. Test properties and testing frequency for high density polyethylene (HDPE) Smooth and Textured Geomembranes. Geosynthetic Institute
39. ASTM International (2015) ASTM D7466. Standard Test Method for Measuring Asperity Height of Textured Geomembranes. In: ASTM International. West Conshohocken, Pennsylvania, USA
40. ASTM International (2021) ASTM D5994. Standard test method for measuring core thickness of textured geomembranes. In: ASTM International. West Conshohocken, Pennsylvania, USA
41. ASTM International (2018) ASTM D1505. Standard test method for density of plastics by the density-gradient technique. In: ASTM International. West Conshohocken, Pennsylvania, USA
42. ASTM International (2020) ASTM D792. Standard test methods for density and specific gravity (relative density) of plastics by

displacement. In: ASTM International. West Conshohocken, Pennsylvania, USA
43. ASTM International (2020) ASTM D6693. Standard test method for determining tensile properties of nonreinforced polyethylene and nonreinforced flexible polypropylene geomembranes. In: ASTM International, West Conshohocken, Pennsylvania, USA
44. ASTM International (2021) ASTM D1004. Standard test method for tear resistance (graves tear) of plastic film and sheeting. In: ASTM International. West Conshohocken, Pennsylvania, USA
45. ASTM International (2020) ASTM D4833. Standard test method for index puncture resistance of geomembranes and related products. In: ASTM International. West Conshohocken, Pennsylvania, USA
46. ASTM International (2020) ASTM D4218. Standard test method for determination of carbon black content in polyethylene compounds by the muffle-furnace technique. In: ASTM International. West Conshohocken, Pennsylvania, USA
47. ASTM International (2021) ASTM D8117. standard test method for oxidative induction time of polyolefin geosynthetics by differential scanning calorimetry. In: ASTM International. West Conshohocken, Pennsylvania, USA
48. ASTM International (2012) ASTM D5321. Standard test method for determining the shear strength of soil-geosynthetic and geosynthetic-geosynthetic interfaces by direct shear. In: ASTM International. West Conshohocken, Pennsylvania, USA